

Glutamine methylation in histone H2A is an RNA-polymerase-I-dedicated modification

Peter Tessarz^{1,2}, Helena Santos-Rosa^{1,2}, Sam C. Robson^{1,2}, Kathrine B. Sylvestersen³, Christopher J. Nelson^{1,2†}, Michael L. Nielsen³ & Tony Kouzarides^{1,2}

Nucleosomes are decorated with numerous post-translational modifications capable of influencing many DNA processes¹. Here we describe a new class of histone modification, methylation of glutamine, occurring on yeast histone H2A at position 105 (Q105) and human H2A at Q104. We identify Nop1 as the methyltransferase in yeast and demonstrate that fibrillarin is the orthologue enzyme in human cells. Glutamine methylation of H2A is restricted to the nucleolus. Global analysis in yeast, using an H2AQ105me-specific antibody, shows that this modification is exclusively enriched over the 35S ribosomal DNA transcriptional unit. We show that the Q105 residue is part of the binding site for the histone chaperone FACT (facilitator of chromatin transcription) complex². Methylation of Q105 or its substitution to alanine disrupts binding to FACT *in vitro*. A yeast strain mutated at Q105 shows reduced histone incorporation and increased transcription at the ribosomal DNA locus. These features are phenocopied by mutations in FACT complex components. Together these data identify glutamine methylation of H2A as the first histone epigenetic mark dedicated to a specific RNA polymerase and define its function as a regulator of FACT interaction with nucleosomes.

Glutamine methylation occurs on translation termination factors and ribosomal proteins³. We investigated whether such a modification exists on histones by interrogating mass spectrometric data sets. We identified a single glutamine, human Q104 (yeast: Q105) in H2A as a site of methylation (Fig. 1a and Extended Data Fig. 1). The residue is located on the surface of the octamer (Extended Data Fig. 2) and is highly conserved in canonical H2A from yeast to human. However, in H2A.Z it is exchanged for a glycine or serine (Fig. 1b). We raised a modification-specific antibody (Extended Data Fig. 3) that detects this modification in yeast and mammalian cells (Fig. 1c).

To identify the methyltransferase responsible, we performed a candidate approach and screened 72 predicted yeast non-essential predicted methyltransferases⁴ by analysing knockout lysates by western blotting with the modification-specific antibody. However, we did not detect loss of signal in any lysate (not shown). We then used an unbiased biochemical approach and fractionated yeast cells as described in Fig. 2a. Fractions were assayed on a 20-residue peptide spanning Q105, or the respective QA mutant, coupled to beads in the presence of tritiated S-adenosyl-methionine (SAM). Methyltransferase activity was assessed by scintillation counting (Fig. 2b) and the fraction containing activity towards H2AQ105 was subjected to mass spectrometry (Supplementary Table 4). All 178 non-essential proteins identified by mass spectrometry were tested by knockout analysis and western blotting, but none showed reduction of Q105 methylation (not shown). We then examined the essential proteins in the active fraction. We focused on Nop1, a known rRNA methyltransferase⁵, because its essential co-factors, Nop56/58 (ref. 6) and other members of an active RNA polymerase I complex⁷ were present in this active fraction. Furthermore, with the exception of Nop58, all the previously

mentioned proteins are known to interact with H2A^{8,9}. Tandem affinity purification (TAP)-tagging of the Nop1 complex purifies an enzymatic activity that methylates H2AQ105 (Fig. 2c). Next, recombinantly purified Nop1 was tested for its ability to modify recombinant H2A *in vitro*. Indeed, Nop1, in the presence of H2A and SAM, methylates H2AQ105 as detected by the H2AQ105me-specific antibody (Fig. 2d and Extended Data Fig. 4a). Additionally, mass spectrometry of this reaction identifies H2AQ105 methylation (Fig. 2e and Extended

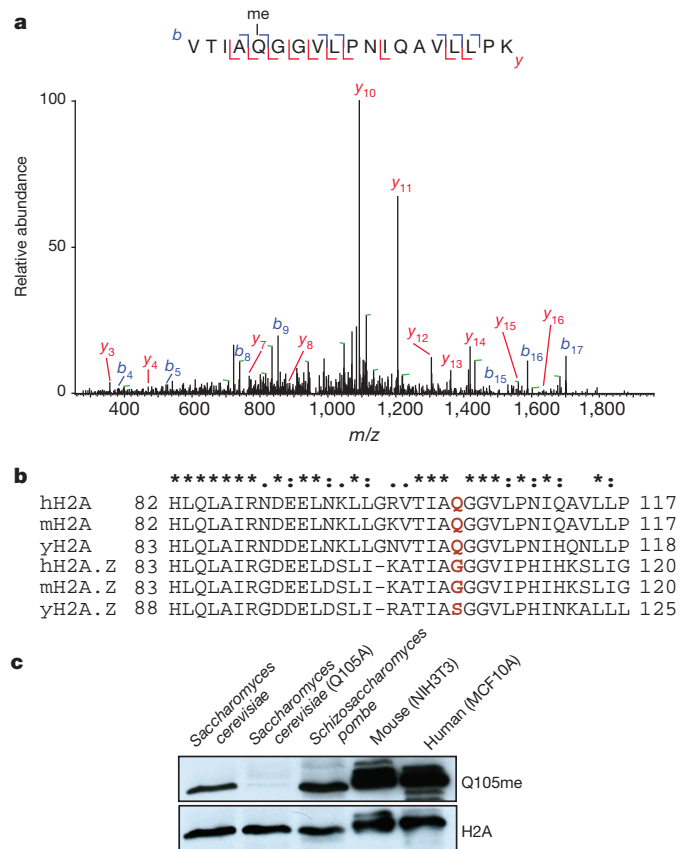


Figure 1 | Identification and localization of methylated H2A glutamine 105. **a**, Tandem mass spectrum of the Q104me modified peptide VTIAQGGVLNIQAVLLPK from H2A. The *y* and *b* series indicate fragments at amide bonds of the peptide, unambiguously identifying the methylated glutamine 104 (in mammalian cells; in yeast, glutamine 105). **b**, Alignment of the region encompassing Q105 of H2A and its variant H2A.Z. Highlighted in red is Q105 in H2A and the corresponding change to glycine or serine in H2A.Z. **c**, Analysis of yeast and mammalian cell extracts for the presence of Q105 methylation using a modification-specific antibody.

¹Gurdon Institute, University of Cambridge, Tennis Court Road, Cambridge CB2 1QN, UK. ²Department of Pathology, University of Cambridge, Tennis Court Road, Cambridge CB2 1QN, UK. ³Department of Proteomics, The Novo Nordisk Foundation Center for Protein Research, Faculty of Health Sciences, University of Copenhagen, Blegdamsvej 3B, DK-2200 Copenhagen, Denmark. [†]Present address: Department of Biochemistry and Microbiology, University of Victoria, 3800 Finnerty Road, Victoria, British Columbia V8P 5C2, Canada.

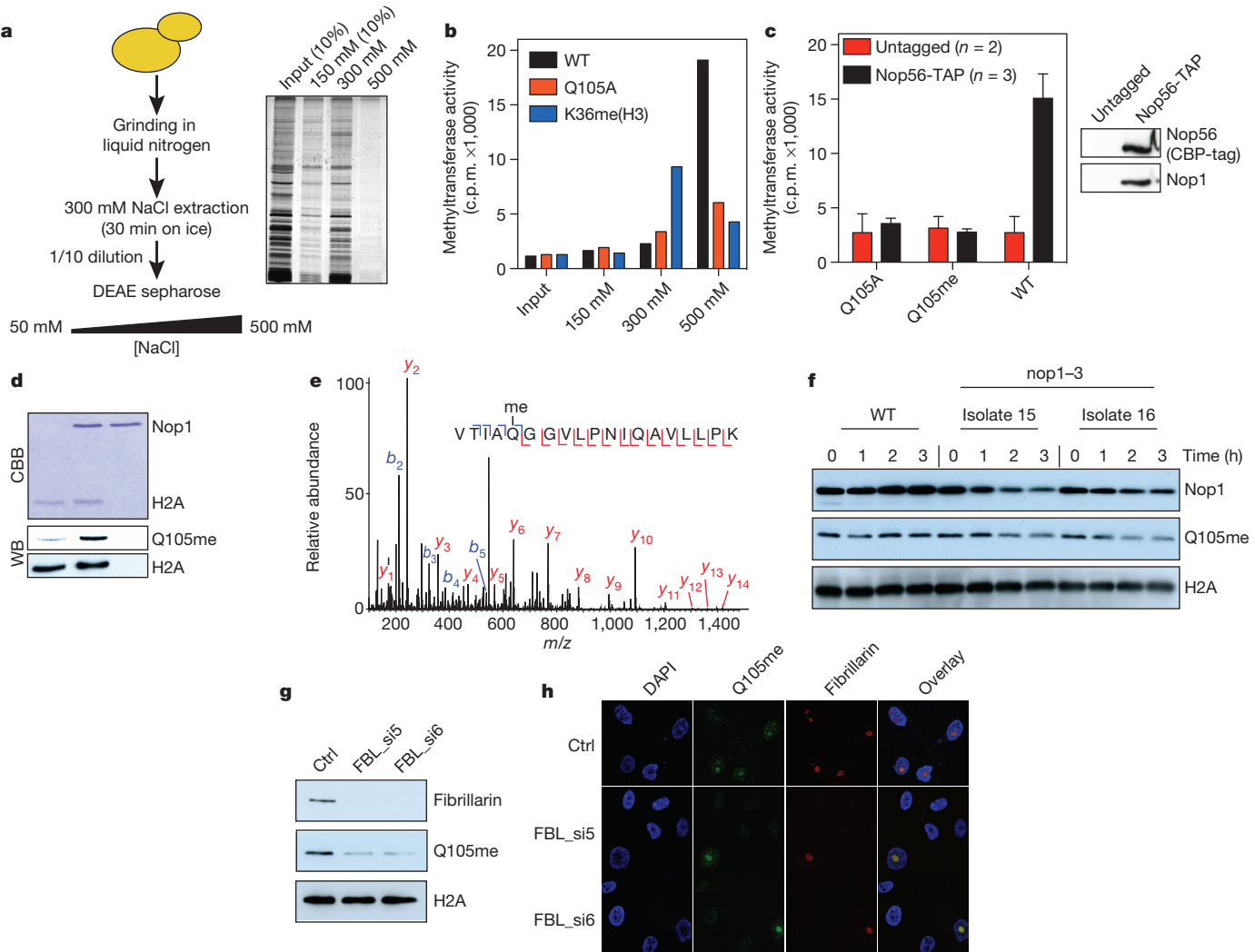


Figure 2 | Identification of Nop1/fibrillarin as the methyltransferase of Q105. **a**, General strategy. **b**, Fractions from **a** were assayed on peptides containing glutamine or alanine at position 105 and compared with an unrelated peptide (H3K36me). For this, peptides were bound to Dynabeads, incubated with extract and tritiated SAM and, after extensive washes, analysed by liquid scintillation. Representative data of three independent experiments are shown. **c**, TAP-tag purification of the Nop1 complex coupled to the same activity assay as in **b** recapitulates the activity as found in the DEAE fraction. **d**, Recombinant Nop1 was incubated with SAM and recombinant histone H2A. Coomassie stain (CBB) and western blot (WB) of the reaction are shown.

e, Tandem mass spectrum of the Q104me modified peptide from H2A, which unambiguously identifies the methylated glutamine 104. **f**, Strains carrying thermosensitive alleles (15 and 16) of Nop1 were analysed for loss of Q105 methylation levels upon shift to restrictive temperature. **g**, The mammalian homologue of Nop1, fibrillarin, was knocked down by independent siRNAs and probed for loss of Q105 methylation 48 h after transfection. A scrambled siRNA served as control (Ctrl). **h**, Immunofluorescence of cells treated as in **g** were stained using the Q105me-specific and anti-fibrillarin antibodies and counterstained with 4',6-diamidino-2-phenylindole (DAPI) as a nuclear marker.

Data Fig. 4b). To test the enzymatic activity of Nop1 *in vivo* we made use of two independently isolated thermosensitive mutants carrying the same amino-acid changes, which are located in the SAM binding site of Nop1 (ref. 5). Yeast harbouring these thermosensitive (*ts*) alleles showed a 50% reduced Q105 methylation signal upon shift to restrictive temperature at a time at which cells are still proliferating (Fig. 2f and Extended Data Fig. 5a, b). These results identify Nop1 as the enzyme responsible for H2AQ105 methylation in yeast.

Nop1 has a single highly conserved homologue in human cells, called fibrillarin¹⁰ (Extended Data Fig. 5c, d). To establish that fibrillarin methylates Q104 in human cells, it was knocked down in MCF10A cells. Transfection of two independent short interfering RNAs (siRNAs) against fibrillarin leads to robustly reduced amounts of H2AQ104me (Fig. 2g and Extended Data Fig. 5e). At this time viability was only marginally affected, based on MTT proliferation assays (Extended Data Fig. 5f). Furthermore, immunofluorescence showed that Q104me and fibrillarin were enriched in the nucleolus of MCF10A cells (Fig. 2h).

However, siRNA-induced knockdown of fibrillarin completely abrogated detection of Q104me in the nucleolus. We observed no morphological changes of the nucleus and nucleolus that have been reported to occur upon prolonged fibrillarin knockdown¹¹, indicating that—in agreement with the MTT assay—the viability of the cells was not affected at the time of analysis.

The main function of the nucleolus is ribosomal DNA (rDNA) transcription and ribosome biogenesis¹². To analyse the distribution of H2A glutamine methylation in chromatin, we performed chromatin immunoprecipitations coupled to deep DNA sequencing (ChIP-seq). The rDNA locus consists of roughly 100–200 repeats in yeast and 200–400 copies in human cells¹³, of which about half are active and almost devoid of nucleosomal structure and the other half are inactive and densely packed with nucleosomes^{13,14}. In yeast up to about 80% of rDNA repeats can be deleted, in which case all the remaining repeats, approximately 20 copies, are active¹⁵. This strain still retains H2AQ105me (Extended Data Fig. 6). Remarkably, when the H2AQ105me antibody

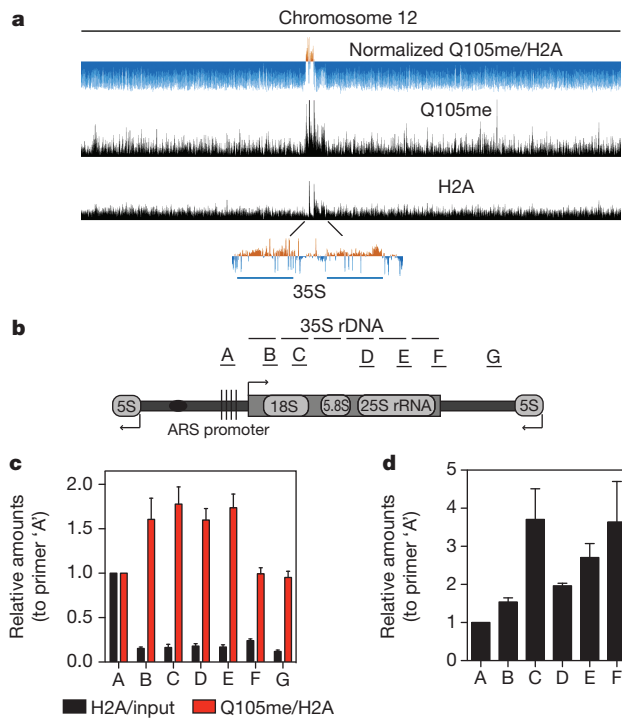


Figure 3 | Genomic landscape of Q105me. **a**, ChIP-seq profile of Q105me and H2A over chromosome 12. The upper plot represents the normalized tracks for the mapped reads of Q105me/H2A. The magnification of the enriched region shows the rDNA region located on this chromosome. The two blue bars represent the 35S transcripts that are present in the genome annotation. **b**, Representation of one rDNA repeat with the position of primers used to scan the rDNA region by ChIP-quantitative (q)PCR. **c**, ChIP-qPCR validation of the ChIP-seq shown in **a**. **d**, Nop1 profile over the rDNA locus. The ChIP-qPCR profile was internally normalized to signal of primer pair 'A'. ChIP-qPCR data show the mean \pm s.e.m. of three independent biological experiments.

is used in ChIP-seq analysis, the only site of enrichment in the entire yeast genome is over the 35S rDNA transcription units (Fig. 3a, c). In addition, Nop1, the enzyme that mediates H2AQ105 methylation, localizes with H2AQ105 methylation at the 35S rDNA locus (Fig. 3d). Together, these results indicate that both in human and in yeast, methylation of H2A represents a modification restricted to the nucleolus. Given the enrichment of glutamine methylation on the transcribed region of the rDNA cluster, we asked whether RNA polymerase I transcription was required for deposition of Q105 methylation. We used actinomycin D at concentrations known to inhibit RNA polymerase I, but not RNA polymerase II¹⁶. These conditions led to reduced Q104/5 methylation in mammalian/yeast cells, indicating that active RNA Pol I transcription is required for glutamine methylation to occur (Extended Data Fig. 7).

Histone methylation can act as a platform to recruit and regulate other chromatin-related factors¹ such as chromatin remodelling complexes. The region spanning Q105 in H2A has previously been described as a potential binding site for FACT^{17,18}, a protein complex consisting of Spt16/Pob3 and Nhp6a in yeast, which is required for efficient passage of RNA and DNA polymerases through chromatin by remodelling nucleosomes². Residues in the region of H2A spanning Q105 show genetic interactions with FACT *ts* mutants^{17,18}, as does a Q105A mutant using a transcription-based reporter system (Extended Data Fig. 8).

To probe the possibility that FACT physically interacts with H2A through the region spanning Q105, we took an unbiased approach (phage display) to identify regions in H2A/H2B interacting with Spt16 and Pob3. A randomized 12-residue peptide phage library was used to enrich for sequences binding to Spt16/Pob3. In line with the published genetic findings, the interaction screen identified a consensus sequence spanning H2AQ105 as the binding site for FACT (Extended Data Fig. 9a).

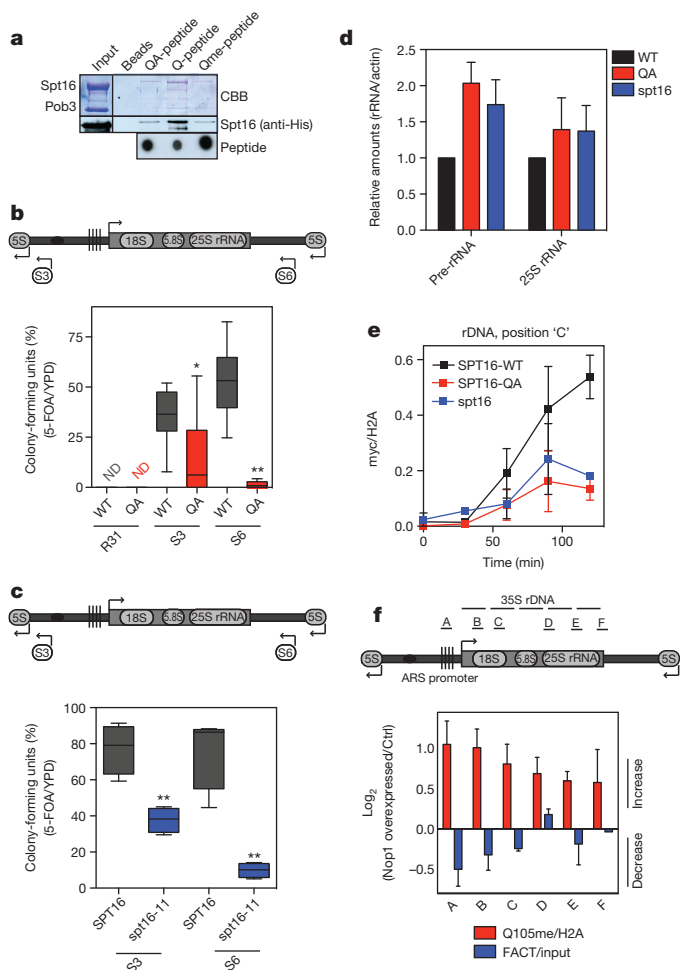


Figure 4 | Unmodified Q105 is part of a recognition motif for FACT. **a**, Indicated peptides were bound to streptavidin-coupled Dynabeads and incubated with recombinantly purified Spt16/Pob3 for 4 h at 4 °C. Input represents 50% of Spt16/Pob3 used for the immunoprecipitations. Bound Spt16/Pob3 was analysed by Coomassie stain (CBB) or western blotting. Peptides were spotted on membrane as loading control. **b**, Effect of the H2AQ105A mutant on the transcription of a *URA3* reporter integrated at the indicated positions in the rDNA repeat (S3 and S6) and R31 outside the rDNA¹⁹. Strains were assayed for their ability to grow on 5-FOA for 3 days at 30 °C ($n \geq 3$; ND, not detected). **c**, The *spt16-11* allele was assayed as described in **c**, but colonies were counted after 1 week. **d**, Yeast expressing either wild-type (WT) or Q105A (QA) mutant H2A as the sole source of histones were assayed for rDNA transcription by transcriptional run-on and compared with cells carrying an *spt16-11* thermosensitive allele (*spt16*). Amounts of RNA are expressed relative to actin. **e**, Differences in histone incorporation rates between WT and Q105A (QA) histones. WT H2A and H2AQ105 were myc-tagged and placed under the control of a galactose-inducible promoter in either wild-type or *spt16-11* cells. Myc-tagged histones were induced by addition of 2% galactose ($t = 0$). Samples were taken at the indicated time points and chromatin immunoprecipitated with anti-myc and H2A antibodies. **f**, Nop1 overexpression (Nop1 overexpressed) leads to an increase of Q105 methylation and a concurrent decrease in FACT occupancy at the rDNA locus. Primer positions are indicated and data presented as the log₂ changes compared with an empty vector control (Ctrl). ChIP-qPCR data show the mean \pm s.e.m. of at least two independent biological experiments. * $P < 0.05$; ** $P < 0.01$.

We next asked whether methylation of H2AQ105 could influence the binding to FACT. Figure 4a shows that binding of recombinant Spt16/Pob3 to a peptide spanning H2AQ105 is significantly decreased when Q105 is methylated or mutated to alanine. Pull-downs from HeLa nuclear extracts using the same peptides demonstrate that the endogenous human FACT complex is responsive to glutamine methylation on H2A (Extended Data Fig. 9b), suggesting that the disruption

of FACT binding to this site is the mechanistic consequence of glutamine methylation.

We next sought to explore the consequence of H2AQ105 methylation on FACT function *in vivo*. To do this, we took advantage of the fact that mutation of H2AQ105 to alanine phenocopies Q105 methylation in terms of effecting FACT binding (Fig. 4a). To study a potential influence of Q105 methylation on rDNA transcription and its interplay with FACT, we turned to a well-established reporter-based system that allows sensitive monitoring of the transcriptional state of the rDNA locus, in which weak, but constitutively expressed, *URA3* cassettes were integrated into the rDNA locus (S3 and S6; Fig. 4b)¹⁹. Figure 4b shows a significant drop in 5-FOA-positive colonies in the Q105A mutant, indicative of a higher transcription rate of the *URA3*. We then introduced the *spt16-11* allele—which leads to a 30–40% decrease in FACT protein levels¹⁷—into the same reporter strains. Figure 4d shows that at semi-permissive temperature we observe a drastic loss of colony numbers on 5-FOA plates, pointing to an increase in transcriptional permissiveness (open chromatin) in accordance with recently published findings²⁰. These results show that reduced FACT activity indeed phenocopies the Q105A mutation. Thus, a mutation that disrupts the function of the chromatin remodeler FACT or a mutation that disrupts the binding of FACT to chromatin lead to transcriptional permissiveness at the rDNA locus. To monitor RNA Pol I transcription rates directly, we performed run-on experiments in wild-type, FACT *ts* and Q105A strains. Figure 4d shows that rDNA transcription was increased using two different primer pairs, confirming a more permissive chromatin at the rDNA locus, when FACT or Q105A are mutated.

One possible explanation for the increased rDNA transcription in the Q105A and FACT *ts* strains, is loss of nucleosomes over a transcribed region. FACT *ts* mutants have already been described as possessing such a phenotype²¹. To investigate a possible histone deposition defect, we generated strains in which we placed myc-tagged versions of either wild-type H2A or the Q105A mutant under control of the *GAL1*-promoter in a wild-type or *spt16-11* yeast background. Induction of the myc-tagged histones was identical as judged by total steady-state levels on western blots (Extended Data Fig. 10a). The wild-type H2A was very efficiently deposited into chromatin as monitored by ChIP (Fig. 4e). However, the *spt16-11* and the Q105A mutant had a profound defect in H2A incorporation into chromatin (Fig. 4e). These findings suggest that methylation of H2AQ105, as phenocopied by the H2AQ105A mutation and a FACT *ts* mutant, results in the transcriptional stimulation of the *URA3* reporters because of reduced nucleosomal occupancy in the rDNA repeat.

Finally, we set out to test directly whether an increase in Q105 methylation on the rDNA locus would decrease FACT occupancy. Indeed, overexpression of Nop1 leads to increased Q105me and is accompanied by a decrease of FACT occupancy, in line with the hypothesis that Q105 methylation is regulating FACT availability on chromatin (Fig. 4f).

The findings presented here identify a new histone modification pathway operational exclusively in the nucleolus. It involves methylation of H2AQ105 by Nop1 in yeast, and methylation of H2AQ104 by fibrillarin in human cells, resulting in the weakening of interactions between H2A and FACT. The FACT complex interacts with all three RNA polymerases^{22,23} and facilitates transcription in two steps by (1) binding and disrupting nucleosomes in the path of the polymerase^{22,24,25} and (2) by augmenting the re-deposition of nucleosomes in the wake of transcribing polymerase^{24,26}. Glutamine methylation of H2A may affect either of these functions by disrupting binding to FACT. The observation that an H2AQ105A mutant is incorporated to a lower extent would favour a model in which re-deposition is decreased. Such a model is also in agreement with earlier observations that rDNA has a low nucleosome occupancy¹³, in contrast to most other regions of the genome. Indeed, recent reports suggest that H2A in particular seems to be depleted from this region²⁷ and that FACT might play a role in this pathway²⁰. The net result of a glutamine-modified chromatin state is that RNA Pol I transits less impeded by nucleosomes. It is worth noting, however, that glutamine methylation of H2A is present in the rDNA locus,

even though deposition is affected. The residual loading of modified H2A might be due to the presence of other histone chaperones such as Nap1 that are insensitive to glutamine methylation on H2A (Extended Data Fig. 10b).

RNA Pol I associates with the Nop1 enzyme and may carry it along during transcription elongation. It is currently unclear how glutamine methylation is initiated or reversed, but it might be linked to the reactivation of the rDNA locus that has been described to occur after DNA replication in an RNA Pol-I-dependent manner²⁷. Another possibility is that the enzyme itself is the key node of regulation. Nop1/fibrillarin is highly modified^{28,29}, so a signalling pathway leading to the glutamine methyltransferase could be the triggering event.

Glutamine methylation of H2A represents the first histone modification that is dedicated to only one of the three RNA polymerases. The selectivity for Pol I and its compartmentalization within the nucleolus might be necessary to generate a chromatin state capable of dealing with the high demands for transcription of ribosomal components. Indeed, glutamine methylation as a whole seems to be a modification that is dedicated to ribosomal biosynthesis: Nop1 has the ability also to methylate rRNA and affect RNA processing⁵; the only other known glutamine methyltransferases in yeast (Mtq1 and Mtq2) modify translational release factors on a conserved glutamine³. Thus, glutamine methylation may have evolved to be a modification dedicated to a specific cellular process. Finally, our finding that a protein can catalyse the methylation of proteins and RNA opens the possibility that many other enzymes may have such dual specificity.

METHODS SUMMARY

The antibody against H2AQ105me was raised using the speedy 28-day programme of Eurogentec using modified peptides coupled to KLH. Yeast genetics, molecular biology, cell culture and biochemistry were performed using standard methods. ChIP was essentially as described earlier³⁰. ChIP-seq was analysed on an Illumina MiSeq. Mapped ChIP-seq reads were normalized by dividing Q105me counts by the H2A counts. Mass spectrometry was performed upon in-gel digest on a LTQ-Orbitrap XL (Thermo Fisher Scientific) and analysed using the MaxQuant software package. Detailed information about the reagents and methodology used is available in Methods.

Online Content Any additional Methods, Extended Data display items and Source Data are available in the online version of the paper; references unique to these sections appear only in the online paper.

Received 9 January; accepted 29 October 2013.

Published online 18 December 2013.

- Kouzarides, T. Chromatin modifications and their function. *Cell* **128**, 693–705 (2007).
- Formosa, T. The role of FACT in making and breaking nucleosomes. *Biochim. Biophys. Acta* **1819**, 247–255 (2012).
- Polevoda, B. & Sherman, F. Methylation of proteins involved in translation. *Mol. Microbiol.* **65**, 590–606 (2007).
- Petrosian, T. C. & Clarke, S. G. Multiple motif scanning to identify methyltransferases from the yeast proteome. *Mol. Cell. Proteomics* **8**, 1516–1526 (2009).
- Tollervey, D., Lehtonen, H., Jansen, R., Kern, H. & Hurt, E. C. Temperature-sensitive mutations demonstrate roles for yeast fibrillarin in pre-rRNA processing, pre-rRNA methylation, and ribosome assembly. *Cell* **72**, 443–457 (1993).
- Gautier, T., Bergès, T., Tollervey, D. & Hurt, E. Nucleolar KKE/D repeat proteins Nop56p and Nop58p interact with Nop1p and are required for ribosome biogenesis. *Mol. Cell. Biol.* **17**, 7088–7098 (1997).
- Fath, S. et al. Association of yeast RNA polymerase I with a nucleolar substructure active in rRNA synthesis and processing. *J. Cell Biol.* **149**, 575–590 (2000).
- Krogan, N. J. et al. Global landscape of protein complexes in the yeast *Saccharomyces cerevisiae*. *Nature* **440**, 637–643 (2006).
- Lambert, J.-P., Mitchell, L., Rudner, A., Baetz, K. & Figeys, D. A novel proteomics approach for the discovery of chromatin-associated protein networks. *Mol. Cell. Proteomics* **8**, 870–882 (2009).
- Jansen, R. P. et al. Evolutionary conservation of the human nucleolar protein fibrillarin and its functional expression in yeast. *J. Cell Biol.* **113**, 715–729 (1991).
- Amin, M. A. et al. Fibrillarin, a nucleolar protein, is required for normal nuclear morphology and cellular growth in HeLa cells. *Biochem. Biophys. Res. Commun.* **360**, 320–326 (2007).
- Raška, I., Shaw, P. J. & Čmarko, D. Structure and function of the nucleolus in the spotlight. *Curr. Opin. Cell Biol.* **18**, 325–334 (2006).
- Albert, B., Perez-Fernandez, J., Léger-Silvestre, I. & Gadal, O. Regulation of ribosomal RNA production by RNA polymerase I: does elongation come first? *Genet. Res. Int.* **2012**, 276948 (2012).

14. Grummt, I. & Längst, G. Epigenetic control of RNA polymerase I transcription in mammalian cells. *Biochim. Biophys. Acta* **1829**, 393–404 (2013).
15. Ide, S., Miyazaki, T., Maki, H. & Kobayashi, T. Abundance of ribosomal RNA gene copies maintains genome integrity. *Science* **327**, 693–696 (2010).
16. Gorenstein, C., Atkinson, K. D. & Falkes, E. V. Isolation and characterization of an actinomycin D-sensitive mutant of *Saccharomyces cerevisiae*. *J. Bacteriol.* **136**, 142–147 (1978).
17. VanDemark, A. P. *et al.* Structural and functional analysis of the Spt16p N-terminal domain reveals overlapping roles of yFACT subunits. *J. Biol. Chem.* **283**, 5058–5068 (2008).
18. McCullough, L. *et al.* Insight into the mechanism of nucleosome reorganization from histone mutants that suppress defects in the FACT histone chaperone. *Genetics* **188**, 835–846 (2011).
19. Smith, J. S. & Boeke, J. D. An unusual form of transcriptional silencing in yeast ribosomal DNA. *Genes Dev.* **11**, 241–254 (1997).
20. Johnson, J. M. *et al.* Rpd3 and Spt16-mediated nucleosome assembly and transcriptional regulation on yeast rDNA genes. *Mol. Cell. Biol.* **33**, 2748–2759 (2013).
21. Hainer, S. J., Pruneski, J. A., Mitchell, R. D., Monteverde, R. M. & Martens, J. A. Intergenic transcription causes repression by directing nucleosome assembly. *Genes Dev.* **25**, 29–40 (2011).
22. Orphanides, G., Wu, W. H., Lane, W. S., Hampsey, M. & Reinberg, D. The chromatin-specific transcription elongation factor FACT comprises human SPT16 and SSRP1 proteins. *Nature* **400**, 284–288 (1999).
23. Birch, J. L. *et al.* FACT facilitates chromatin transcription by RNA polymerases I and III. *EMBO J.* **28**, 854–865 (2009).
24. Belotserkovskaya, R. *et al.* FACT facilitates transcription-dependent nucleosome alteration. *Science* **301**, 1090–1093 (2003).
25. Winkler, D. D., Muthurajan, U. M., Hieb, A. R. & Luger, K. Histone chaperone FACT coordinates nucleosome interaction through multiple synergistic binding events. *J. Biol. Chem.* **286**, 41883–41892 (2011).
26. Formosa, T. *et al.* Defects in SPT16 or POB3 (yFACT) in *Saccharomyces cerevisiae* cause dependence on the Hir/Hpc pathway: polymerase passage may degrade chromatin structure. *Genetics* **162**, 1557–1571 (2002).
27. Wittner, M. *et al.* Establishment and maintenance of alternative chromatin states at a multicopy gene locus. *Cell* **145**, 543–554 (2011).
28. Choudhary, C. *et al.* Lysine acetylation targets protein complexes and co-regulates major cellular functions. *Science* **325**, 834–840 (2009).
29. Wang, B., Malik, R., Nigg, E. A. & Körner, R. Evaluation of the low-specificity protease elastase for large-scale phosphoproteome analysis. *Anal. Chem.* **80**, 9526–9533 (2008).
30. Santos-Rosa, H. *et al.* Methylation of histone H3 K4 mediates association of the Isw1p ATPase with chromatin. *Mol. Cell* **12**, 1325–1332 (2003).

Supplementary Information is available in the online version of the paper.

Acknowledgements We thank E. Hurt, D. Stillman, T. Kobayashi, J. Smith and J. Boeke for providing strains; K. Lilley for mass spectrometry and M. Vermeulen for help with identifying H2AQ104me; S. Moss for running the Illumina MiSeq; members of the Kouzarides laboratory for discussions; and A. Bannister and R. Belotserkovskaya for reading the manuscript. This work has been financed by a programme grant from Cancer Research UK and a project grant from the Biotechnology and Biological Sciences Research Council (BB/K017438/1).

Author Contributions P.T. and H.S.-R. designed experiments, performed research, interpreted data and wrote the manuscript. K.B.S. and M.L.N. performed mass spectrometry. C.J.N. supplied new reagents. T.K. designed experiments, interpreted data and wrote the manuscript.

Author Information Data of the ChIP-seq experiments have been deposited in Array Express under accession number E-MTAB-1447. Reprints and permissions information is available at www.nature.com/reprints. The authors declare competing financial interests: details are available in the online version of the paper. Readers are welcome to comment on the online version of the paper. Correspondence and requests for materials should be addressed to T.K. (t.kouzarides@gurdon.cam.ac.uk).

METHODS

Strains, plasmids and reagents. Genotypes of strains and yeast plasmids used in this work are listed in Supplementary Table 1. If not stated otherwise, all strains used were derivatives of W303. Integrations and deletions were performed using one-step PCR-based methods^{31,32}. All plasmids used were verified by sequencing. Non-radioactive SAM and recombinant histones were purchased from New England Biolabs and tritiated SAM from Perkin Elmer. Peptides for immunization were from ChemPep and biotinylated peptides were from Cambridge Peptides using Fmoc-Gln(Me)-OH (ChemPep). Ni-NTA and IgG Sepharose were from GE Healthcare, amylose resin from New England Biolabs and streptactin-sepharose from iBA. Streptavidine, protein A and protein G Dynabeads were from Invitrogen. D-Desthiobiotin was purchased from Sigma and Factor Xa from New England Biolabs. FlexiTube siRNA was from Qiagen (FBL_5: 5'-ACACTTTGTGATTTTC CATTAA-3'; FBL_6: 5'-ATCGTTGGTCCGGATGGTCTA-3') and siRNA transfection reagent RiboCellin was from BCC. Protease inhibitors were from Roche. DMEM-H/F12, penicillin-streptomycin-fungizone and epidermal growth factor were from Invitrogen and cholera toxin from List Biological Laboratories. Insulin and hydrocortisone were from Sigma. MTT assays were purchased from Invitrogen. Alpha factor was from GenScript and pronase from Calbiochem.

Antibodies. The Q105me antibody was produced using the Eurogentec Speedy 28-day polyclonal package. Sera were purified using unmodified and modified peptide columns and tested for specificity (Extended Data Fig. 3). Anti-H2A (ab13923 for Fig. 1c) mouse anti-fibrillarin (ab4566 for immunofluorescence), rabbit anti-fibrillarin (ab5821 for western blot) and mouse anti-HA (ab1424) were from Abcam. Anti-myc (9E10 for ChIP), rabbit anti-c-myc (C3956 for western blot), anti-biotin (B7653) and anti-Flag (M2) were from Sigma and anti- γ H2A (39235) and anti-H3K56Ac (61061) were from Active Motif. Anti-CBP tag (K-24), anti-SSRP1 (D-7) and anti-Spt16 (H-4) were from Santa Cruz. All antibodies were used as suggested by the supplier; anti-H2AQ105me was diluted 1:10,000 for western blotting, 1:50 for ChIPs and 1:100 for immunofluorescence.

Protein purification. Proteins were expressed in BL21 Codon Plus. For FACT, Spt16 and Pob3 were cloned into the pDuet series of Novagen. Cells were grown in Luria Bertani medium (LB) to $D_{600\text{nm}} = 1$ at 37 °C. Cells were then shifted to 20 °C for one hour before induction with 1 mM IPTG overnight. Cells were lysed in buffer A (20 mM HEPES-KOH pH 7.5, 50 mM KCl, 20 mM imidazole, 5 mM β-mercaptoethanol, 10% glycerol) supplemented with 1 mg ml⁻¹ lysozyme. Cells were lysed using six 30-second pulses on a Branson Sonifier. The lysate was centrifuged and supernatant was bound to 1 ml Ni-NTA for 2 h at 4 °C. The matrix was washed with 100 ml buffer A and eluted in the same buffer supplemented with 250 mM imidazole. The eluate was bound to 2 ml streptactin-sepharose for 2 h at 4 °C. Subsequently, the matrix was washed using 100 ml buffer A and Spt16/Pob3 were eluted in the same buffer containing 2.5 mM D-desthiobiotin.

Nop1 was expressed in BL21 Codon Plus as a maltose-binding-protein fusion and purified using the pMal System (New England Biolabs) according to the manufacturer's protocol. Nop1 was eluted off the matrix by Factor Xa cleavage. The protein was polished over a Resource S column and a linear gradient from 150 to 500 mM NaCl.

H2A and derivatives were purified as described³.

Activity assays. For peptide-based activity assays, peptides (5 mg ml⁻¹) were bound to streptavidine-coated M280 beads (20 µl of slurry and 1.6 µl peptide per reaction) and incubated for 1 h at room temperature in TBS/0.1% NP40. Beads were washed several times to remove unbound peptide. For the reaction, the equivalent of 20 µl of beads were distributed into microtubes. Fifty microlitres of extract (see below) and 1 µl tritiated SAM were added, and incubated at 30 °C for 30 min. Subsequently, 1 µl of tritiated SAM was added and the reaction was incubated for another 30 min. Beads were washed three times with 200 µl TBS/0.1% NP40 and once in 200 µl TBS/1 M NaCl/0.1%NP40. Beads were resuspended in 200 µl TBS/0.1% NP40 and boiled for 5 min. One hundred microlitres of supernatant were counted in a scintillation counter.

For assays on recombinant H2A, 0.2 µg of Nop1 was assayed on 1 µg of recombinant H2A in the presence of 100 µM SAM in ½ TBS and 1 mM dithiothreitol (DTT) for 30 min at 30 °C. Half of the reaction was loaded on SDS-polyacrylamide gel electrophoresis for Coomassie staining and 2% of the reaction for western blotting.

Extract preparation for activity assays and mass spectrometry. Three litres of yeast were grown to $D_{600\text{nm}} \sim 0.6$. The cell pellet was washed twice with ice-cold PBS. The pellet was resuspended in 2× volume of nuclear lysis buffer (10 mM Tris pH 8, 420 mM NaCl, 2 mM EDTA, 10% glycerol, 0.1% NP40, 1 mM DTT) supplemented with protease inhibitors. Small droplets were made into liquid nitrogen. Cells were lysed by grinding on liquid nitrogen in a mortar for 10–15 min. The powder was thawed quickly at 30 °C and put back on ice for 10 min. The cell lysate was centrifuged for 2 min at 2,500g in a tabletop centrifuge at 4 °C to remove unbroken cells. This crude lysate was extracted for another 30 min on ice before centrifuging it for 10 min at 20,000g at 4 °C. The supernatant was diluted into

10 mM Tris, 5 mM MgCl₂, 10% glycerol, 1 mM DTT and bound to a 1 ml equilibrated DEAE column. The column was washed with 10 column volumes and proteins were step eluted with 150 mM, 300 mM, 500 mM and 1000 mM NaCl (500 µl fractions). The fractions were dialysed overnight in 10 mM Tris, 150 mM NaCl, 5 mM MgCl₂, 10% glycerol, 1 mM DTT and used for activity assays. The fraction containing the activity was run on SDS-polyacrylamide gel electrophoresis and processed for liquid chromatography-tandem mass spectrometry at the Cambridge Centre for Proteomics, Department of Biochemistry, University of Cambridge. Protein hits were identified using Mascot software.

Extracts for TAP-tag purification were generated as described above. The cleared lysate was then incubated with 200 µl IgG Sepharose beads for 2 h at 4 °C and treated as described for the original TAP-tag protocol. Briefly, the beads were washed with 30 ml of IPP150 and 10 ml of tobacco etch virus (TEV)-cleavage buffer, followed by TEV cleavage at 4 °C overnight.

Peptide pull-downs. For peptide immunoprecipitations, 15 µl of the respective peptides (at 5 mg ml⁻¹) were diluted in 200 µl TBS/0.1% NP40 and incubated with an equivalent of 100 µl of equilibrated slurry for 1 h at room temperature. Beads were washed twice with 1 ml TBS/0.1% NP40, and washed beads were incubated with 1 µg of Spt16/Pob3 (10 nM final) in 500 µl TBS/0.1% NP40, 1 mM DTT for 2 h at 4 °C. Subsequently, beads were washed four times with 1 ml TBS/0.1% NP40 1 mM DTT and eluted with 50 µl SDS-sample buffer.

Phage display assay. We used the Ph.D.-12 Phage Display Peptide Library Kit from New England Biolabs to screen for a potential Spt16/Pob3 interaction site in H2A using the manufacturer's instructions. As a bait we used His6-tagged Spt16/StrepII-Pob3. In the first selection round we used Ni-NTA, in the second streptactin and in the third round we used both matrices for affinity purification. DNA of enriched phages was prepared and sequenced using the kit's primer.

ChIP. Chromatin was sonicated to produce fragments of 400–500 base pairs (bp). ChIP was performed essentially as described³⁰, except ChIPs for H2AQ105me, in which case five times more chromatin was used as input. Real-time PCR used a StepOnePlus system with Fast SYBR Green (Applied Biosystems). Standard curves for each primer set were calculated from amplification of diluted DNA. After each run, a dissociation curve was performed to ensure that no primer dimers contaminated the quantification and that the product had the expected melting temperature. Each PCR reaction was performed in duplicate and the signal intensity value for each sample was calculated from the average of the two experiments. Primer sequences are shown in Supplementary Table 2. Relative fluorescent intensities for the ChIP experiments were calculated as follows: (Ab signal – IgG signal)/(input signal – IgG signal), where Ab is the antibody of interest, IgG is the negative control antibody and input the sheared genomic DNA. Each experiment was repeated between two and four times from independent cultures.

ChIP-seq. Fifty per cent of a ChIP reaction was used to generate the library. Library production followed the protocol published on <http://ethanomics.wordpress.com/chip-seq-library-construction-using-the-illumina-truseq-adapters/> (2012) with few changes. Purification steps using AMPure XP beads were replaced by the ChIP DNA Clean & Concentrator kit by ZymoResearch. Illumina adaptors were exchanged for Bioo Nextflex adaptors 1–3 (1:100 dilution each). Size selection was performed on a SAGE Pippin Prep using 2% gels and selecting for a size between 350 and 600 bp. The quality of the library was assessed using Agilent DNA High Sensitivity ChIPs and Qiagen Qubit. Libraries were pooled and sequenced on an Illumina MiSeq using single-ended 50 bp reads.

Transcriptional run-on. Nuclear Run-On was performed essentially as described earlier³³. Briefly, cells were inoculated to a starting absorbance ($A_{600\text{nm}}$) of approximately 0.03 and grown in YPAD medium to $A_{600\text{nm}} \sim 0.1$ –0.15. Five $A_{600\text{nm}}$ units of culture (approximately 5×10^7 cells) were collected by centrifugation at 3,000g for 3 min. Cells were resuspended in 5 ml of ice-cold H₂O and then centrifuged at 4 °C for 3 min at 3,000g. The cells were then re-suspended in 950 µl of ice-cold H₂O, and 50 µl of 10% sarkosyl was added. The sample was gently mixed and incubated on ice for 20 min. The permeabilized cells were pelleted by microcentrifugation for 1 min, and the supernatant was carefully removed. Residual supernatant was removed after a second brief microcentrifugation.

The cells were suspended in 97.5 µl of transcription buffer (50 mM Tris hydrochloride (pH 8), 100 mM KCl, 5 mM MgCl₂, 1 mM MnCl₂, 2 mM DTT) supplemented with 40 U of RNase OUT (Invitrogen). Reactions were started by adding 2.5 µl of RNA biotin labelling mix (Roche) and shifting to 30 °C. After 5 min the reaction was pipetted into a fresh Eppendorf tube with 250 µl glass beads and 1 ml TRIzol reagent (Invitrogen) on ice. Cells were lysed and homogenized by bead beating for 4 × 1 min with incubation on ice for 3 minutes in between. After the last vortexing, the reactions were incubated at room temperature for 5 min followed by RNA extraction after the TRIzol. The RNA pellet was resuspended in 200 µl of 10 mM Tris-HCl (pH 7.5), 1 mM EDTA, 100 mM NaCl, and 50 µl of washed T1-streptavidine-coupled Dynabeads were added for 2 h at room temperature. Beads were washed twice in 500 µl of 2× SSC (1× SSC is 0.15 M NaCl plus

0.015 M sodium citrate), 15% formamide for 15 min and once in 500 µl of 2× SSC for 5 min. Beads were resuspended in 12 µl RNase free water and RNA was reverse transcribed. Sequences of primers used for qPCR are given in Supplementary Table 2.

Sequence mapping. Called reads from the Illumina MiSeq system were mapped to the latest version of the *Saccharomyces cerevisiae* genome (sacCer3) using Burrows Wheeler Aligner with parameters -n 10, -k 3, -l 20 (ref. 34). PCR duplicates mapping to identical regions on the genome were removed using SamTools³⁵. Filtered mapped reads were extended to the fragment length of 400 bp and converted to wiggle format using the bedTools suite of utilities³⁶. Raw and mapped reads are given in Supplementary Table 3.

Normalization. Extended reads were counted in bins of 50 bp across the entire genome and were normalized to the total number of mapped reads for each sample to account for differences in read depth. Within each bin, the level of Q105me enrichment above H2A control was determined by first subtracting the IgG read count and subsequently thresholding at a minimum value of one (adjusted value). The normalized Q105me count was generated by dividing the adjusted Q105me values by the adjusted H2A count. Data were transformed to a log₂ scale for visualization.

Western blot. Western blots of total yeast extracts were performed by standard procedures. Transfers to nitrocellulose membranes were made on carbonate buffer (21.1 g l⁻¹ NaHCO₃, 18.35 g l⁻¹ Na₂CO₃, pH 9.5) at 45 mA for 70 min. The membranes were blocked for 1 h at room temperature in TBS + 0.1% Tween-20 + 5% BSA; primary antibody was incubated at 4 °C overnight and secondary antibody for 1 h at room temperature.

Cell culture. MCF 10A (CRL-10317) cells were obtained from the American Type Culture Collection and were grown in DMEM-H/F12 medium supplemented with 1% penicillin-streptomycin-fungizone, 10 µg ml⁻¹ insulin, 100 ng ml⁻¹ cholera toxin, 20 ng ml⁻¹ epidermal growth factor, 500 ng ml⁻¹ hydrocortisone and 5% FBS at 37 °C in 5% CO₂ humidified atmosphere. NIH-3T3 were grown in DMEM supplemented with PenStrep and 5% FBS at 37 °C in 5% CO₂ humidified atmosphere.

Transfections of siRNA were done according to the manufacturer's instructions. For 10 cm dishes, 750,000 cells were seeded and transfected 24 h later. For any other dish, cell numbers were adjusted to area. MTT assays were performed according to the manufacturer's protocol.

Immunofluorescence. Cells were processed for immunofluorescence as described earlier³⁷, but primary antibody incubation was overnight at 4 °C. Images were acquired using an Olympus FV1000 upright system equipped with a ×60/1.35 UPlanSApo Oil and a ×100/1.40 UPlanSApo Oil objective. Images were processed further using ImageJ software.

In-gel digestion. Proteins were resolved on 4–20% SDS-polyacrylamide gel electrophoresis. The gel was stained with colloidal Coomassie blue, cut into 20 slices and processed for mass spectrometry as previously described³⁸. Briefly, cysteines were reduced with DTT, alkylated using chloroacetamide³⁹, digested overnight with trypsin and loaded onto StageTips before mass spectrometry⁴⁰.

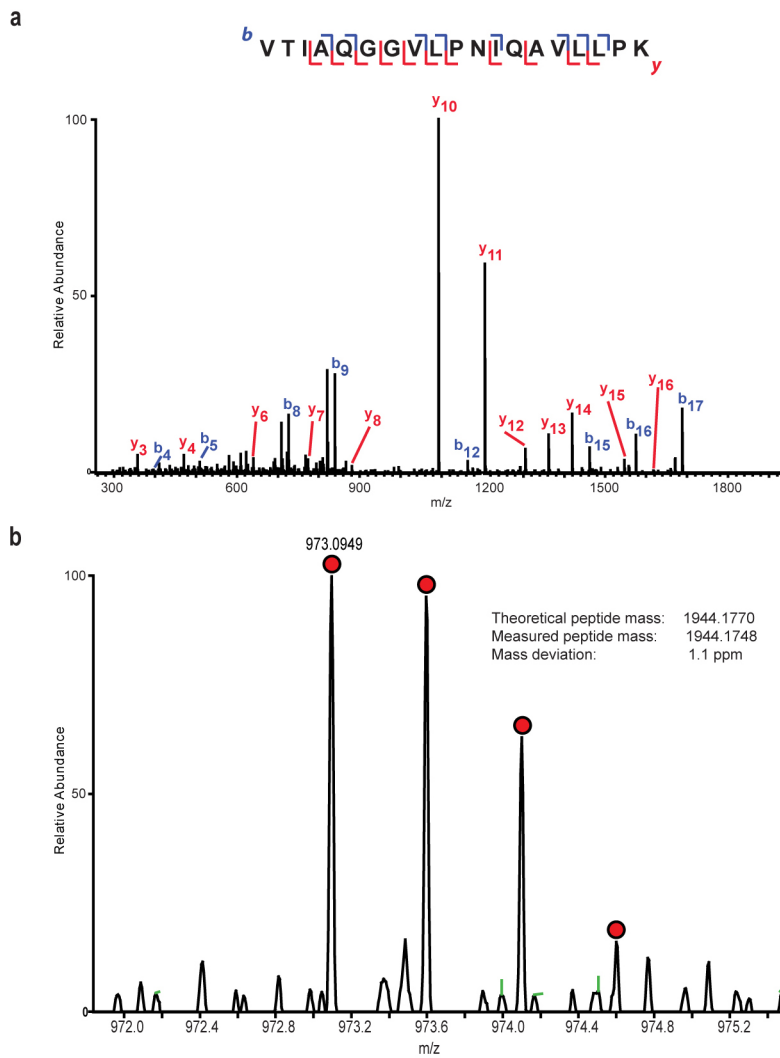
Mass spectrometry. All mass spectrometric experiments were performed on a nanoscale high-performance liquid chromatography system (EASY-nLC from Thermo Fisher Scientific) connected to a hybrid LTQ-Orbitrap XL (Thermo Fisher Scientific) equipped with a nanoelectrospray source. Each peptide sample was separated on a 15 cm analytical column (75 µm inner diameter) packed in-house with 3 µm C18 beads (Reprosil Pur-AQ, Dr Maisch) with a 2 h gradient from 5 to 40% acetonitrile in 0.5% acetic acid. The eluate from the high-performance liquid chromatography was directly electrosprayed into the mass spectrometer. The mass spectrometric instrument was operated in data-dependent mode to switch automatically between full-scan mass spectrometry and tandem mass spectrometry acquisition. Survey full-scan mass spectrometric spectra (from *m/z* = 300–1,800) were acquired in the Orbitrap analyser with resolution *R* = 60,000 at *m/z* = 400

after accumulation to a 'target value' of 1,000,000 in the linear ion trap using 'Top10' method. The ten most intense peptide ions with charge states of at least 2 were sequentially isolated to a target value of 3,000 using automatic gain control and fragmented by collisional induced dissociation in the linear quadrupole ion trap (LTQ).

Identification of peptides and proteins by MaxQuant. The data analysis used MaxQuant software (version 1.2.7.1, www.maxquant.org) as described⁴¹, supported by Andromeda as the database search engine for peptide identifications⁴². Tandem mass spectrometric peak lists were generated by filtering spectra to contain at most six peaks per 100 thomsons interval and subsequently searched by Andromeda against a concatenated target/decoy (forward and reversed) version of the Uniprot human database (68,079 forward protein entries). Protein sequences of common contaminants such as human keratins and proteases were added to the database. The initial mass tolerance in mass spectrometry mode was set to 7 p.p.m. and in tandem mass spectrometry was 0.5 thomsons. Cysteine carbamidomethylation was set as a fixed modification, whereas protein N-acetylation, glutamine methylation and oxidized methionine were set as variable modifications. A maximum of two missed cleavages were allowed while we required strict tryptic specificity. All top-scoring peptide assignments made by Andromeda were filtered based on previous knowledge of individual peptide mass error. Peptide assignments were statistically evaluated in a Bayesian model on the basis of sequence length and Andromeda score as described⁴³. Only peptides and proteins with a false discovery rate of less than 1% were accepted, estimated on the basis of the number of accepted reverse hits.

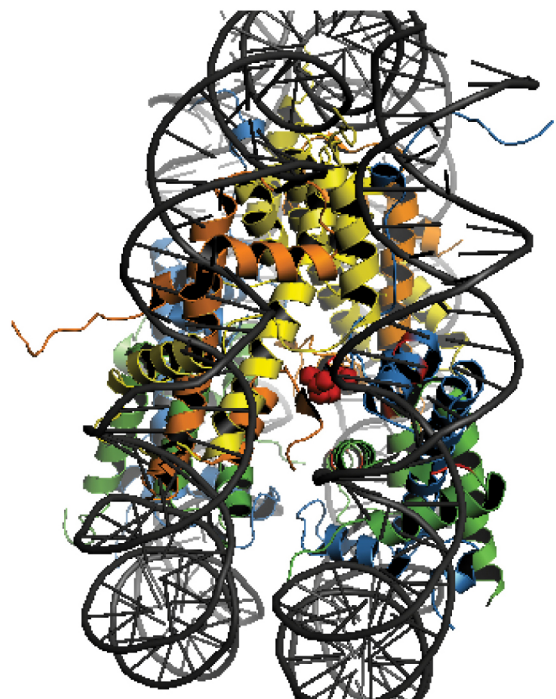
Statistics. Average (mean) and s.e.m. were calculated in Prism (Graphpad) and statistical significance based on Student's *t*-test (always two-tailed) in Microsoft Excel. All experiments were performed at least in triplicate (biological replicates). **P* < 0.05; ***P* < 0.01.

31. Janke, C. et al. A versatile toolbox for PCR-based tagging of yeast genes: new fluorescent proteins, more markers and promoter substitution cassettes. *Yeast* **21**, 947–962 (2004).
32. Longtine, M. S. et al. Additional modules for versatile and economical PCR-based gene deletion and modification in *Saccharomyces cerevisiae*. *Yeast* **14**, 953–961 (1998).
33. Patrone, G. et al. Nuclear run-on assay using biotin labeling, magnetic bead capture and analysis by fluorescence-based RT-PCR. *BioTechniques* **29**, 1012–1014, 1016–1017 (2000).
34. Li, H. & Durbin, R. Fast and accurate short read alignment with Burrows-Wheeler transform. *Bioinformatics* **25**, 1754–1760 (2009).
35. Li, H. et al. The Sequence Alignment/Map format and SAMtools. *Bioinformatics* **25**, 2078–2079 (2009).
36. Quinlan, A. R. & Hall, I. M. BEDTools: a flexible suite of utilities for comparing genomic features. *Bioinformatics* **26**, 841–842 (2010).
37. Bartke, T. et al. Nucleosome-interacting proteins regulated by DNA and histone methylation. *Cell* **143**, 470–484 (2010).
38. Shevchenko, A., Wilm, M., Vorm, O. & Mann, M. Mass spectrometric sequencing of proteins silver-stained polyacrylamide gels. *Anal. Chem.* **68**, 850–858 (1996).
39. Nielsen, M. L. et al. Iodoacetamide-induced artifact mimics ubiquitination in mass spectrometry. *Nature Methods* **5**, 459–460 (2008).
40. Rappaport, J., Ishihama, Y. & Mann, M. Stop and go extraction tips for matrix-assisted laser desorption/ionization, nanoelectrospray, and LC/MS sample pretreatment in proteomics. *Anal. Chem.* **75**, 663–670 (2003).
41. Cox, J. & Mann, M. MaxQuant enables high peptide identification rates, individualized p.p.b.-range mass accuracies and proteome-wide protein quantification. *Nature Biotechnol.* **26**, 1367–1372 (2008).
42. Cox, J. et al. Andromeda: a peptide search engine integrated into the MaxQuant environment. *J. Proteome Res.* **10**, 1794–1805 (2011).
43. Cox, J. et al. A practical guide to the MaxQuant computational platform for SILAC-based quantitative proteomics. *Nature Protocols* **4**, 698–705 (2009).

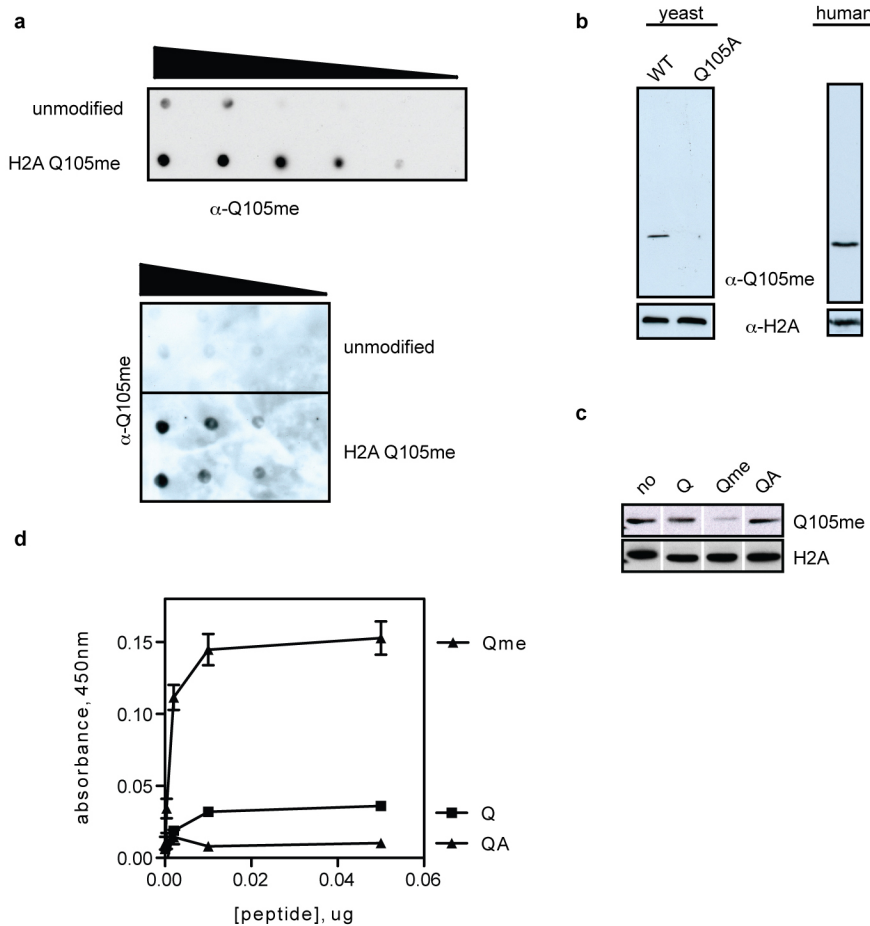

Extended Data Figure 1 | Mass spectrometry of histone H2A.

a, Tandem mass spectrum of the unmodified peptide sequence VTIAQGGVLPNIQAVLLPK from histone H2A. The spectrum correlates with the Q104me modified spectrum presented in Fig. 1a. **b**, Isotope cluster of

Q104me modified peptide VTIAQGGVLPNIQAVLLPK from H2A. Using high-resolution mass spectrometry ensures that peptides are identified with an accuracy of parts per million.

**Extended Data Figure 2 | Position of H2AQ105 in the nucleosome.**

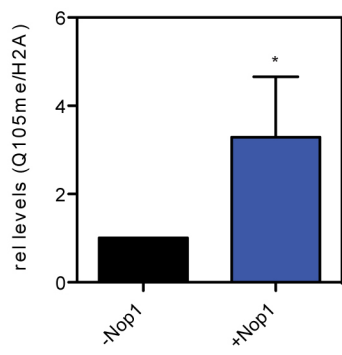
Structure of the yeast nucleosome (1ID3). Q105 is highlighted as a red sphere, localized at the surface of the histone octamer without contacting the DNA, but it is part of the interface between H2A and H3. H3 is in yellow, H4 in orange, H2A in blue and H2B in green.



Extended Data Figure 3 | Quality control of the H2A Q105me antibody.

a, Examples of dot blots of dilution series (1:2) of unmodified or methylated peptide spotted on 0.22 μ m PVDF membrane and developed using the anti-H2A Q105me antibody. **b**, Left, western blot on lysates of cells harbouring either WT or Q105A H2A as sole source of histones; right, human lysate from MCF10A cells. All western blots were probed with the anti-H2AQ105me-specific antibody or anti-H2A upon stripping, respectively. **c**, Peptide competition by western blotting with the indicated peptides shows that only the

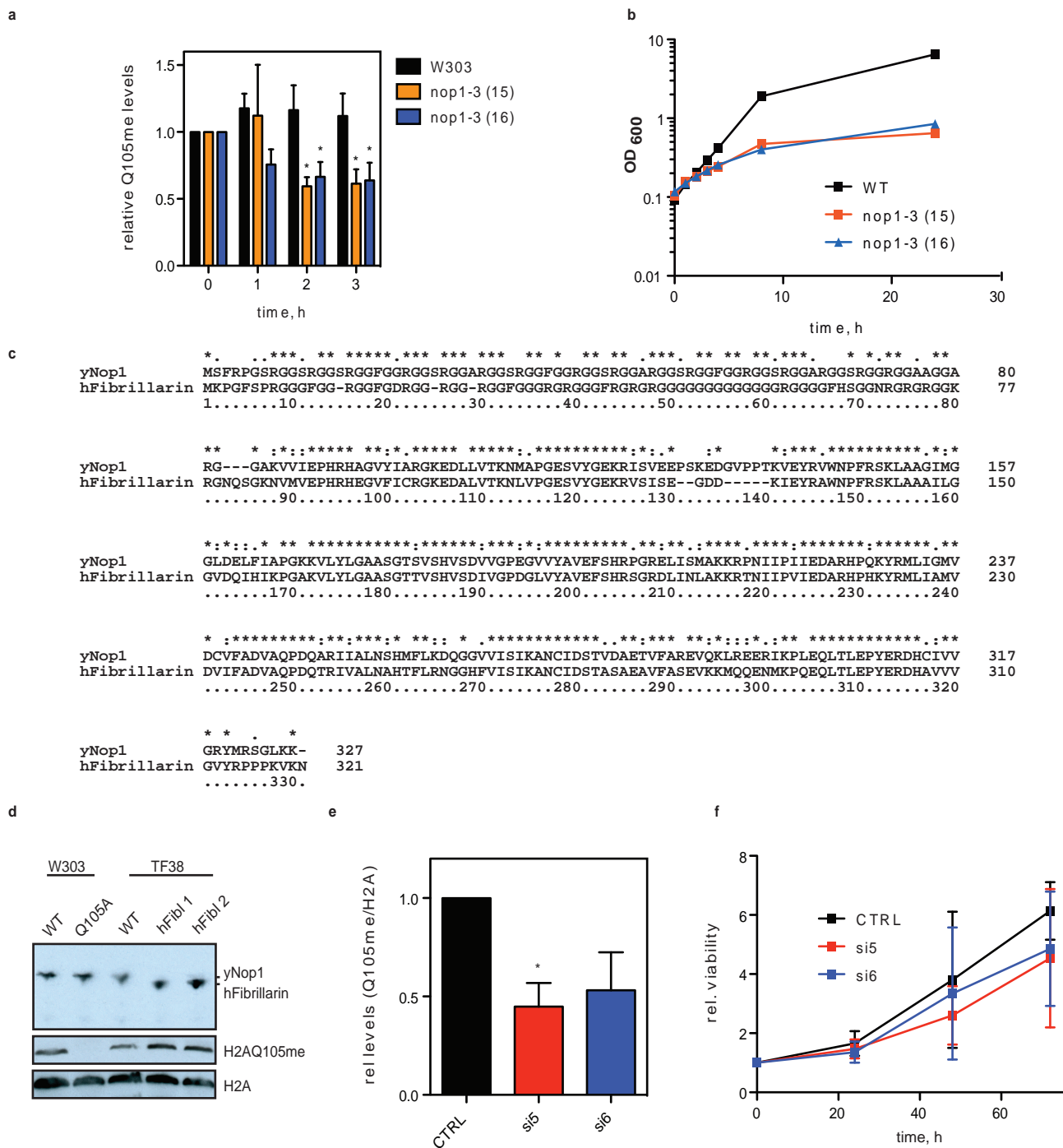
methylated peptide can compete the signal of MCF10A lysates (peptide concentration was at 1 μ g ml $^{-1}$). **d**, Direct enzyme-linked immunosorbent assay (ELISA) against the indicated peptides. Biotinylated peptides were immobilized on streptavidine-coated 96-well plates and the ELISA was performed using a 1:20,000 dilution of the anti-Q105me antibody. The ELISA was developed using horseradish peroxidase (HRP)-coupled secondary anti-rabbit antibody and 3,3', 5,5''-tetramethylbenzidine (TMB) as substrate.

a**b**

b-ion	Theo. Mass	Obs. Mass	ppm
b2	201.1239	201.1231	3.98
b3	314.208	314.2067	4.14
b4	385.2451	385.2434	4.41
b5	527.3193	527.3168	4.74
y-ion	Theo. Mass	Obs. Mass	ppm
y1	147.1134	147.1126	5.44
y2	244.1661	244.1652	3.69
y3	357.2502	357.2490	3.36
y4	470.3342	470.3330	2.55
y5	569.4027	569.4014	2.28
y6	640.4398	640.4384	2.19
y7	768.4984	768.4968	2.08
y8	881.5824	881.5808	1.81
y9	995.6253	995.6238	1.51
y10	1092.6781	1092.6766	1.37
y11	1205.7622	1205.7618	0.33
y12	1304.8306	1304.8256	3.83
y13	1361.8520	1361.8541	-1.54

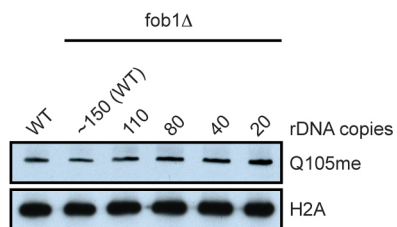
Extended Data Figure 4 | Western blot quantification of *in vitro* methylation reaction and detailed fragmentation table. **a**, Quantification of five independent *in vitro* methylation reactions. Western blots were scanned and intensities were determined using ImageJ. * $P < 0.05$. **b**, Theoretical and

measured *b*- and *y*-ion fragment masses for Q104 methylation of human H2A (peptide sequence VTIAQGGVLPNIQAVLLPK) for mass spectrum shown in Fig. 2e.

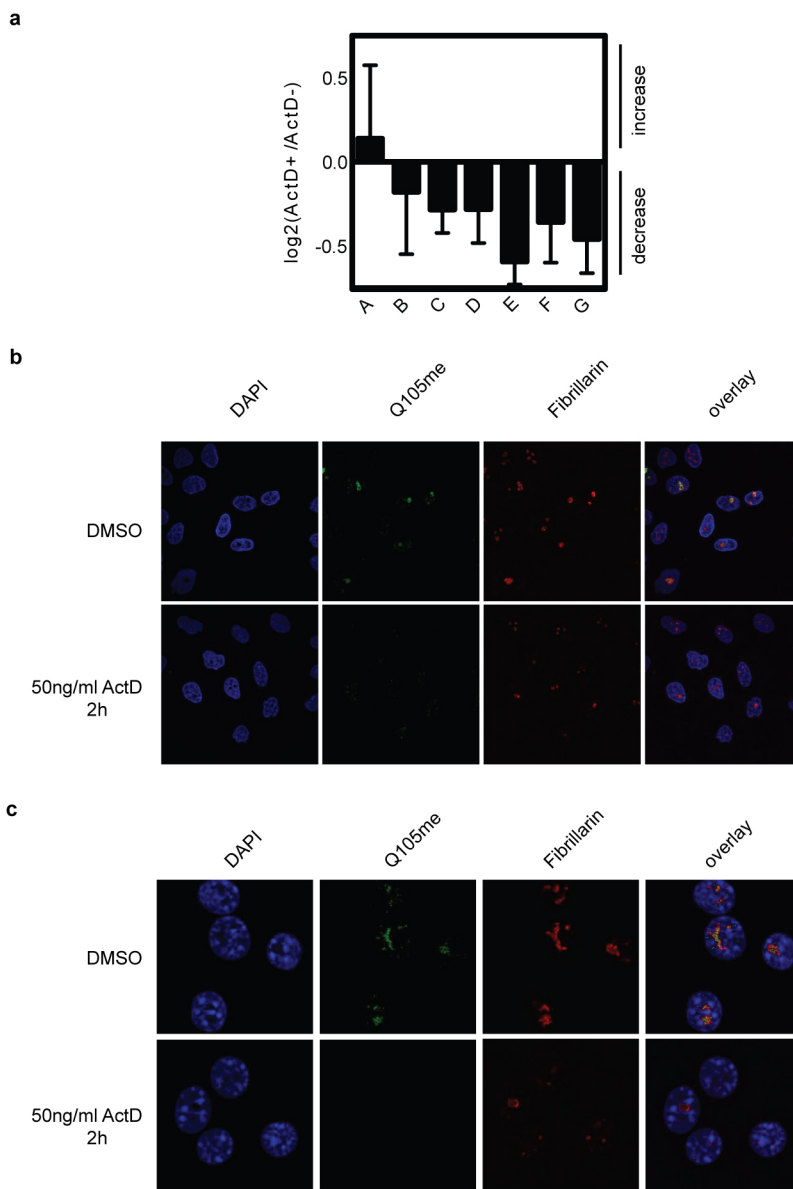


Extended Data Figure 5 | Western blot quantification and growth curves for Nop1/fibrillarin depletion. **a**, Quantification of western blots for Fig. 2f. Here, the average band intensities of three independent experiments were determined using ImageJ and plotted. The amounts of H2AQ105me were expressed as relative levels at time point $t = 0$. * $P < 0.05$. **b**, Growth curve of WT and *nop1.3 ts* strains upon shift to restrictive temperature. **c**, Alignment of yeast Nop1 and its mammalian orthologue fibrillarin indicates that both proteins share

around 70% identity. **d**, Human fibrillarin is able to replace yeast Nop1 to methylate H2AQ105 *in vivo*. Note that human fibrillarin migrates slightly faster than yeast Nop1. **e**, Quantification of western blots for Fig. 2g. Here, the average band intensities of three independent experiments were determined using ImageJ and plotted. * $P < 0.05$. **f**, MTT assays of MCF10A cells transfected with scrambled RNA interference or RNA interference directed against fibrillarin (si5 and si6).



Extended Data Figure 6 | Deletion of rDNA copies does not affect H2AQ105me. The deletion of rDNA copies in yeast (as indicated in the figure) does not decrease the level of Q105me within the cells. Extracts from yeast isogenic yeast strains harbouring different numbers of rDNA repeats were subjected to western blotting and probed with the anti-Q105me and anti-H2A antibodies respectively.

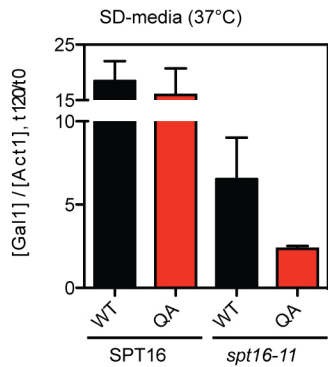
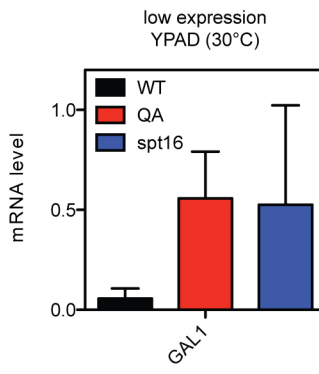
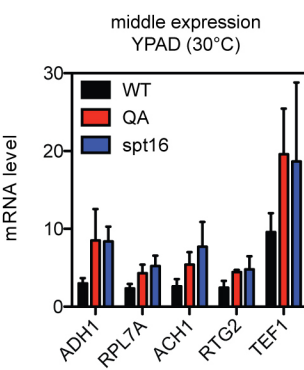
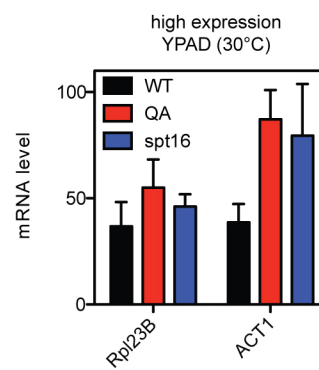


Extended Data Figure 7 | Actinomycin D treatment leads to loss of Q104/5me in cells. **a**, Logarithmically growing yeast cells were treated with 500 ng ml⁻¹ actinomycin D (ActD+) or dimethylsulphoxide (ActD-) for 2 h before fixation. ChIP against Q105me and H2A was analysed with the indicated primer sets and the ratio treated/untreated (showing either an increase or

decrease in treated/untreated samples) was plotted in \log_2 scale. **b**, MCF10A cells were treated with either dimethylsulphoxide or 50 ng ml⁻¹ actinomycin D for 2 h specifically to shut down RNA polymerase-I-mediated transcription. Cells were fixed and processed for immunofluorescence with the indicated antibodies/dyes. **c**, As in **b**, but with NIH-3T3 cells.

a

MSGGKGGKAGSAAKASQSRSAKAGLTFPVGRVHRLRRGNYAQRIGSGAPVYLAVLEYLAAEILEL
 AGNAARDNKKTRIIPRHLQLAIRNDDELNKLLGNTVIAQGGVLVPNIHQNLLPKKSAKATKASQEL

b**c****d****e**

Extended Data Figure 8 | Genetic interaction of spt16-11 and H2AQ105A. **a**, Sequence of H2A with highlighted residues that genetically interact positively (light blue,¹⁷ or negatively (green)¹⁸ with FACT thermosensitive mutations. H2AQ105 (red) is part of this region. **b**, Analysis of wild-type H2A or H2AQ105A in either wild type (SPT16) or thermosensitive mutations (*spt16-11*) with respect to their effect on the induction of a FACT-dependent gene (*GAL1*). Cells were grown in Raffinose-containing media overnight, diluted into Raffinose-containing media and allowed to grow to mid-logarithmic phase before shifting them to restrictive temperature for 4 h. Gal1 was induced by addition of 2% galactose (final). Samples were taken before and 120 min after induction. The relative ratio of *GAL1*-mRNA levels of three independent experiments is given. Also note that this assay is artificial as

Q105me is not detected at the *GAL1* locus in wild-type strains and is only intended to show a potential genetic interaction between H2AQ105me and FACT if they occur at a given genomic location. It is important to note that *GAL1* is an inducible gene and different functions of FACT are required for inducible and steadily expressed genes. The activation of promoters requires the removal of nucleosomes whereas constitutive transcription relies on both removal and re-deposition. To understand the differences between these two FACT functions, we looked at the steady-state level of (c) low, (d) mid- and (e) high constitutively expressed genes at 30 °C. Interestingly, in contrast to inducible genes, many constitutive genes show increased transcription in Q105A and *spt16*, in agreement with a more open chromatin state.

a

VRHMAPHRIAAQGGG
 VRHMAPHRIAAQGGG
 VRHMAPHRIAAQGGG
 VRHMAPHRIAAQGGG
 SMPAPFHAIMQVGGG

 GGWTNLPNPHTIGGG
 GGWTNLPNPHTIGGG

 VWGSHHQRRIVNGGG
HQRHLFNSTTYGGG

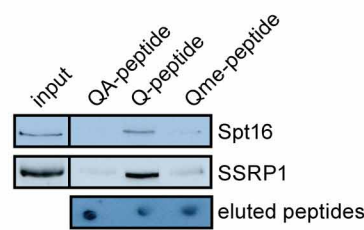
HTA1

MSGGKGGKAGSAAKASQSRSAGL
 TFPVGRVHRLRRGNYAQRIGSGAP
 VYLTAVLEYLAAEFILELAGNAARDN
 KKTRIIIPRHLQLAIRNDDELNKLLG
 NVTIAQGGVLPNIHQNLPKSAKA
 TKASQEL

HTB1

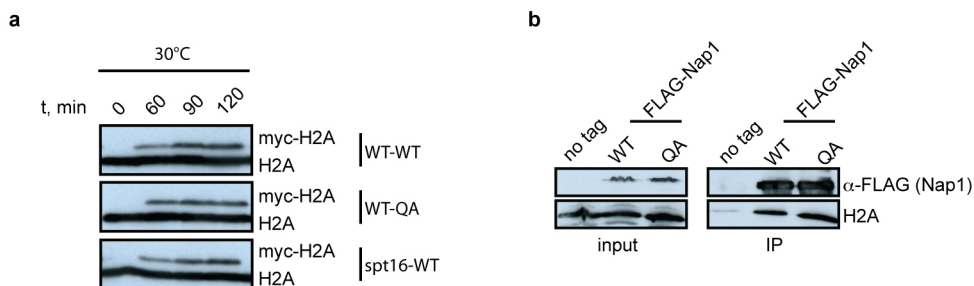
SNAHMQKYTVGLGGG
 VCALHTPMQILSGGG
 TRLVDNPNHLRGGG
 GAFDGCYSQYFWWRG
 LPGRAHD PWKVPGGG
 SLPGRADPWKVPGGG
 ASGTHSHRSPTWGGG
 HRRHLFNFNTTYGGG

MSAKAEKKPASKAPAEKKPAAKKTS
 TSTDGKKRSKARKETYSSYIYKVLK
 QTHPDGTGISQKSMSILNSFVNDFE
 RIATEASKLAAYNKKSTISAREIQT
 AVRLILPGELAKHAVSEGTRAVTKY
 SSSTQA

b**Extended Data Figure 9 | FACT binds to a region spanning H2AQ105.**

a, Left, the peptides enriched in a phage display screen using recombinant Spt16/Pob3 as bait; right, a putative consensus binding sequence (red). **b**, The interaction between Q105 and FACT and the influence of its methylation are

conserved from yeast to mammalian cells. HeLa nuclear extract was incubated with the indicated peptides bound to streptavidin-coupled Dynabeads. Bound proteins were analysed by western blotting.



Extended Data Figure 10 | Influence of H2AQ105A on Nap1 binding.
a, The induction kinetics for Gal1-driven H2A in wild-type and *spt16* mutant cells, as well as H2AQ105A, is identical. Cells were treated as in Fig. 4f and samples were taken at the indicated time points and analysed by western

blotting. **b**, H2A Q105 is not required for interaction with the histone chaperone Nap1. Flag-tagged Nap1 was used to immunoprecipitate either wild-type H2A or the Q105A mutant H2A. An untagged wild-type strain served as background control.